Effects of Tensile Prestrain on the Notch Toughness of Low-Alloy Steel

J.H. CHEN, Z. LI, and G.Z. WANG

Tensile prestrains of various levels were applied to blank steel specimens. Four-point bend tests of notched specimens at various temperatures revealed an appreciable drop in the notch toughness of the specimens, which experienced 3 pct tensile prestrain. Further prestrains of up to 20 pct had a negligible effect on the notch toughness despite additional increases in the yield strength. Microscopic analyses combined with finite element method (FEM) calculations revealed that the decrease in toughness resulted from a change of the critical event controlling the cleavage fracture. The increase in yield strength provided by prestraining allowed the normal tensile stress at the notch tip to exceed the local fracture stress σ_f for propagating a just-nucleated microcrack. As a result, for the coarse-grained steel with low σ_f tested presently, the critical event was changed from tensile stress-controlled propagation of a nucleated microcrack to plastic strain-controlled nucleation of the microcrack at the notch tip. A reduction of toughness was induced as a result of this. The increase in yield strength provided by decreasing the test temperature acted in the same way.

I. INTRODUCTION

MOST early work revealed that prestrain results in deterioration of toughness of steels, as evidenced by decreasing fracture toughness, increasing transition temperature, and inducing cleavage at low stress.[1–7]

In contrast, some work revealed the following.

(1) Lorenz[8] found that prestrain did not affect the plasticity or toughness of steels, and for drawn wire, the toughness increased with drawing strain.
(2) In the authors' work investigating the effects of warm prestressing on the apparent toughness of high-strength low-alloy steel, it was found that the local fracture stress σ_f was not affected by the prestressing up to yielding.[9,10]

Some questions remain regarding the effects of prestrain as well as the mechanism controlling fracture under such conditions.

This work focuses on the effects of tensile prestrain on the notch toughness of deliberately coarsened low-alloy steel and the mechanism of these effects from the viewpoint of changes of the critical event for cleavage fracture.

II. EXPERIMENTAL

A. *Materials and Specimens*

Composition of the steel is shown in Table I. It is a clean steel with an elaborate refining process. Two types of heat treatments were carried out on the steel for obtaining desired microstructures and grain sizes. One was to heat the steel to 1000 °C for 6 hours, followed by a furnace cool. The microstructure, designated CG, contains ferrite grains with about 7 pct pearlite colonies and a few carbide particles, as shown in Figure 1. The histograms of size distributions of ferrite grains, pearlite colonies, and carbide particles are shown in Figure 2. The largest grain size corresponds to those in the coarse grain region of the welding heat-affected zone (HAZ) with a heat input of 3 kJ/mm. For comparison, the second heat treatment consisted of 945 °C/45 min, followed by a furnace cool. The grain sizes are finer and the microstructure is designated as FG. Related histograms are shown in Figures 3 and 4. As shown by these figures, the sizes of microstructures of both steels are much larger than those of conventional steels, even though the microscopic sizes of FG are smaller than those of CG. The deliberately coarsened grain microstructures and subsequent prestraining were adopted for simulating the thermal-strain behavior of the coarse grain region in the welding HAZ with a heat input of 3 kJ/mm.

B. *Specimens*

Four-point bending (4PB) specimens were cut in the L-T direction. The dimensions of blank single and double notch specimens are shown in Figure 5 in the manner used by previous researchers.[24–26,28] Before the notches were cut, some blank specimens were uniformly loaded to various tensile prestrain levels at room temperature.

The dimensions of tensile test specimens are shown in Figure 6.

C. *Mechanical Tests*

1. *Prestrained procedure*

Blank 4PB test specimens and tensile test specimens were loaded in tension at a crosshead rate of 2 mm/min by a universal test machine Shimadzu (Japan) AG-10T at room temperature. Prestrains up to 20 pct were applied. The prestrains were assessed by the formula $\ln (F/F_0)$, where the F is the area measured and averaged at three cross sections after tensile loading. The F_0 is the corresponding area before loading.

2. *Tensile and 4PB test*

Tensile specimens without prestrains were tested at various temperatures from −196 °C to room temperature. Tensile specimens with various prestrains were tested at −100 °C, −125 °C, and −196 °C. 4PB specimens were tested at −100 °C, −125 °C, and −196 °C. The yield strength σ_y was measured by the tensile test, and the stress-strain curve was

J.H. CHEN and G.Z. WANG, Professors, are with State Key Laboratory of New Nonferrous Metal Materials, Gansu University of Technology, Gansu, 730050, P.R. China. Contact e-mail: zchen@gsut.edu.cn Z. LI, Doctorate Student, is with Dalian University of Science and Engineering, Mechanical Engineering Institute, Dalian 116000, P.R. China.

Manuscript submitted May 20, 2002.

Table I. Compositions of Used Steel (Weight Percent)

C	Mn	Si	Mo	Cr	V	S	P	B
0.06	1.36	0.23	0.21	0.19	0.03	0.009	0.020	0.0017

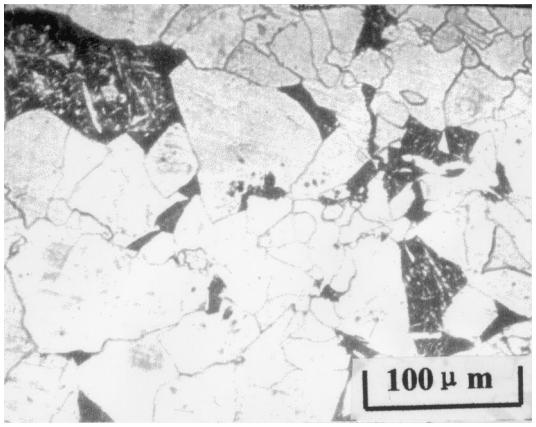

Fig. 1—Microstructure of CG.

digitized and fit into the series of data for finite element method (FEM) calculation. The general yield load P_{gy} of the 4PB specimen was calculated with the formula

$$P_{gy} = 1.155 C_f \sigma_y B (W - a)^2 / 2L$$

where 1.155 is the von Mises parameter, C_f is the constraint factor 1.22, B is the thickness, W is the height, a is the notch depth, and $L = 12.7$ mm is the bending span. The terms B and W are actual measured values. Because all blank specimens subjected to tensile prestrain shrank in the two traverse directions, the actual measured values of B and W were less than the original ones and different for each individual specimen. The notches of specimens were cut with the same depth $a = 4.25$ mm for all specimens. The actual measured values of σ_y, W, and B were used to calculate P_{gy} by the preceding formula. All of values of σ_y, W, B, and calculated P_{gy} are listed in Tables V through VIII.

D. *Microscopic Observation*

Fracture surfaces of all specimens were observed in detail with a scanning electron microscope S-520 made by Hitachi (Japan). The initiation site of cleavage fracture was located by tracing the river pattern strips back to their origin with the similar method used by previous researchers.[23–27] The distance of the cleavage initiation site from the tip of the blunted notch was measured as X_f. For specimens with fibrous cracking prior to cleavage, the length of the fibrous crack was measured. For doubly notched specimens, metallographic sections perpendicular to the surviving notch root were made in the manner used by previous researchers[24–27] to observe the remaining crack and identify the critical event of cleavage.

E. *FEM Calculation*

The stress and strain distributions ahead of notches were calculated for 4PB specimens tested at various temperatures.

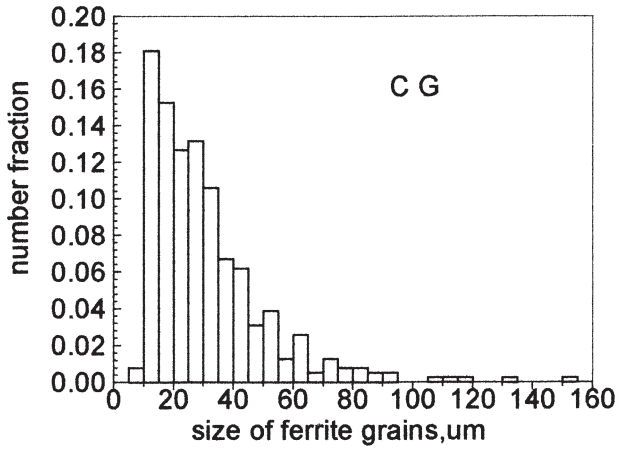

(*a*)

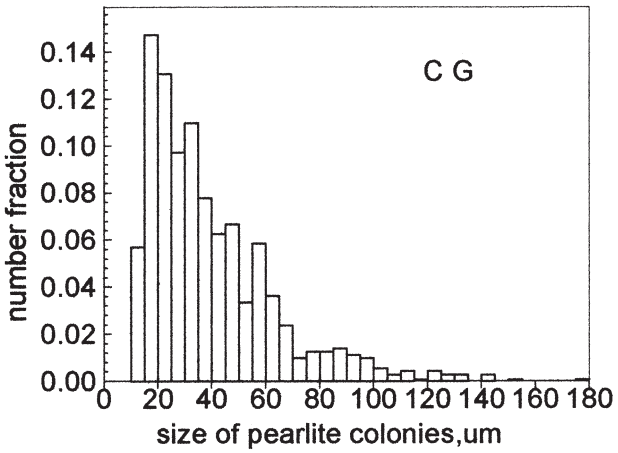

(*b*)

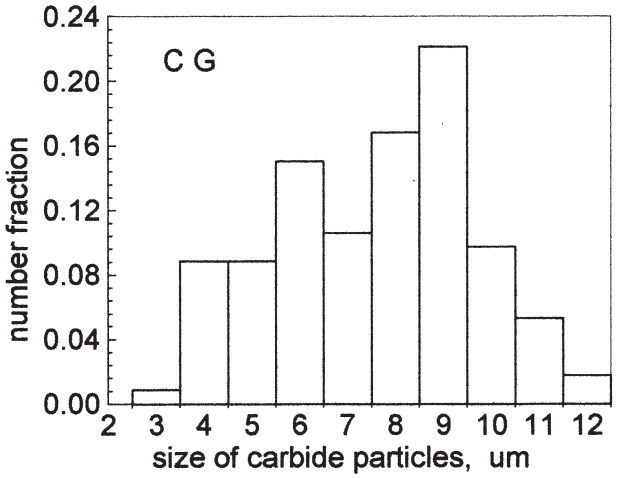

(*c*)

Fig. 2—Histograms of size distributions of (*a*) ferrite grains, (*b*) pearlite colonies, and (*c*) carbide particles of CG microstructure.

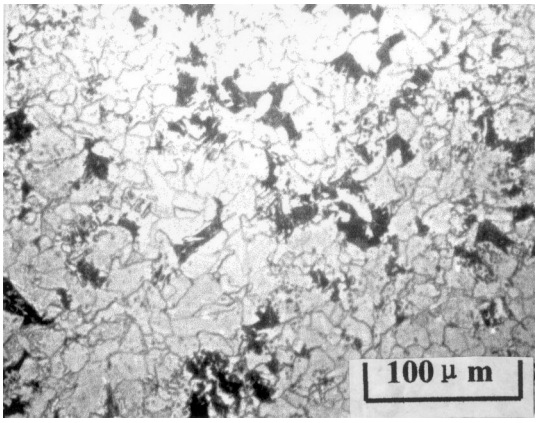

Fig. 3—Microstructure of FG.

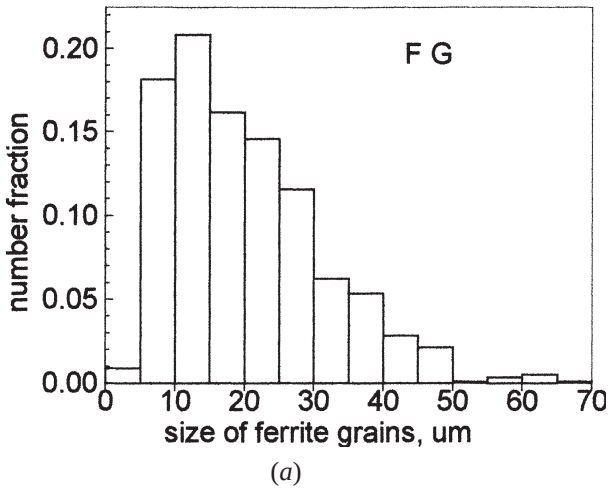

(*a*)

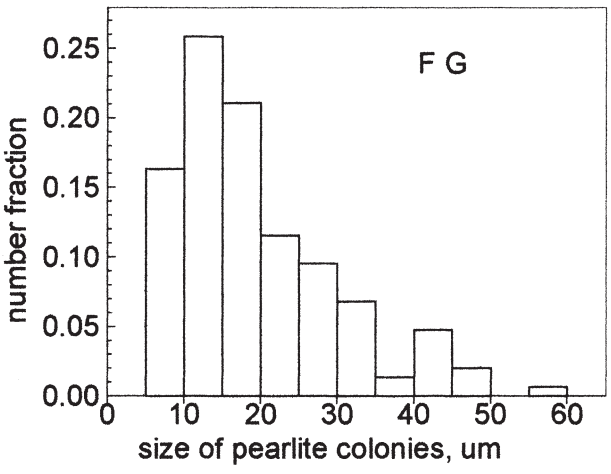

(*b*)

Fig. 4—Histograms of size distributions of (*a*) ferrite grains and (*b*) pearlite colonies of FG microstructure.

These calculations was conducted to complement previous analyses on these types of specimens, which utilized linear hardening and different rates of power law hardening.[28,29]

A two-dimensional model with eight-node biquadratic plane strain reduced integration elements (CPE8R) was used with the ABAQUS code. Ten elements were uniformly distributed around the notch root. A power-law hardening $\sigma = K\varepsilon^n$ was used for the elastic-plastic model.

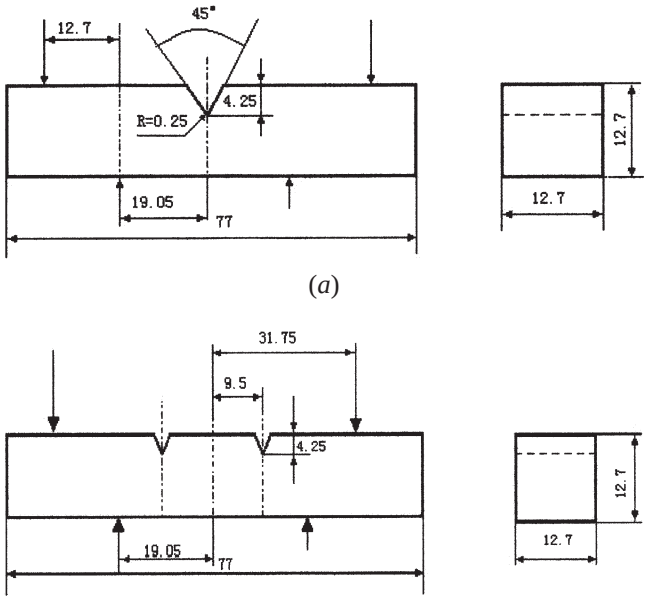

(*a*)

(*b*)

Fig. 5—Dimensions of 4PB test specimens with (*a*) single notch and (*b*) double notches.

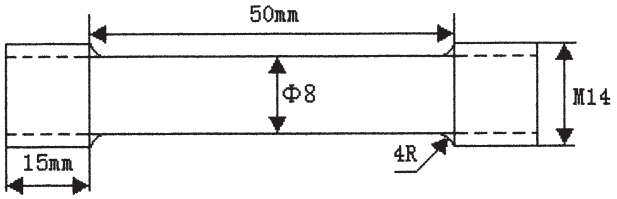

Fig. 6—Dimensions of tensile test specimens.

To simplify the calculation, the mechanical parameters used in the FEM calculation were those measured in the prestrained specimens and averaged over a range of prestrains, as shown in Table II.

Details of the FEM mesh and assessment of the FEM calculation are presented in Appendix I. In Appendix II, a figure compares the results calculated with specimen dimensions shown in Figure 5(a) and with specimen dimensions after 20.5 pct prestrain (no. 709). From Appendix II, it is found that the variation in the specimen's dimensions has a negligible effect on the calculated values when the results are given in terms of P/P_{gy}. Thus, the original specimen's dimensions shown in Figure 5(a) were used for FEM calculations through this work.

III. RESULTS

A. *Results of Mechanical Tests*

1. *Results of tensile tests*

The results of the tensile tests of specimens for the CG and FG steels with various prestrains are shown in Table III and IV, respectively. As shown in Tables III and IV, increasing

the level of prestrain increases the yield strength σ_y for both microstructures.

2. *Results of 4PB tests*

Figures 7 and 8 summarize the variations of notch toughness (characterized by the ratio of fracture load to general yield load, P_f/P_{gy}) at various test temperatures against the level of prestrain for CG and FG steels, respectively. For both microstructures at a temperature of −125 °C (and −100 °C for CG), an appreciable drop in notch toughness of specimens that experienced 3 pct tensile prestrain was observed. Further prestrain had a negligible effect on the notch toughness even though the yield strength still increased. At a test temperature of −196 °C, the effect of prestrain was much less significant and was obscured by the scatter of values measured at various levels of prestrain.

Table II. Mechanical Parameters Used for FEM Calculation

Material	T (°C)	ε_{po} (Pct)	n_p	K_p
CG	−100	0	0.215	974
		0 to 10	0.122	842
		10 to 20	0.042	779
CG	−125	0	0.171	750
		0 to 10	0.127	934
		10 to 20	0.045	822
CG	−196	0	0.046	979
		0 to 10	0.035	1278
		10 to 20	0.025	1123
FG	−125	0	0.107	946
		0 to 6	0.098	892
		6 to 10	0.067	855
		10 to 20	0.020	850
FG	−196	0	0.048	1075
		0 to 10	0.033	1077
		10 to 14	0.030	1130
		14 to 20	0.027	1155

ε_{po} = prestrain, n_p = plastic part of hardening exponent, and K_p = plastic part of constant in formula $\sigma = K_p\varepsilon_p^n$.

B. *Results of Microscopic Observation*

The parameters measured on the fracture surfaces are summarized in Tables V through VIII. The following observations are obtained from the data of Tables V through VIII.

(1) The majority of "zero values" of X_f, the distance from the cleavage initiating site to the notch root, are exhibited by specimens that experience prestrain. In this case, cleavage is initiated at or very close to the notch tip, as shown in Figure 9. This is a characteristic of a crack-nucleation-controlling mechanism.
(2) In some specimens without prestrain (009, 011, and 012 for CG; 503, 505, and 602 for FG), fibrous cracks emanating from the notch occur before cleavage initiation. In metallographic sections of fractured doubly notched specimens without prestrain, grain-sized (017) or pearlite colony-sized (604) remaining cracks were found (Figure 10) in front of the surviving notch. Similar features have been reported in References 24, 26, and 30. These cracks indicate that the normal tensile stress is not sufficient to propagate the just nucleated microcrack in a cleavage manner and indicate a crack-propagation-controlled mechanism.

In Tables V and VII, the variations of P_{gy} were caused by the variations of dimensions of individual specimens, which are also shown in Tables V through VIII.

Table III. Properties Measured in Specimens of CG with Various Tensile Prestrains

Number	T (°C)	ε_{po} (Pct)	σ_y (MPA)	σ_b (MPa)	σ_f (MPa)	ψ (Pct)	K_p (MPA)	n_p
L22	−28	0	288	470	1259	76	856	0.237
L21	−60	0	311	—			813	0.214
L19	−100	0	402	563	1164	70	915	0.215
L20	−125	0	467	—				
L23	−196	0	789	—	872	7.4	942	0.036
L24	−196	0	804	—	857	4.6	1013	0.056
L25	−196	0	787	—	881	7.2	982	0.047
L08	−100	2.5	498	566	1149	68	833	0.130
L05	−100	5.0	545	598	1185	67	834	0.105
L07	−100	9.8	583	619	1209	67	860	0.100
L11	−100	14.4	626	638	1168	65	773	0.048
L16	−100	18.5	651	658	1170	64	766	0.035
L03	−125	3.0	521	606	1213	67	922	0.145
L06	−125	5.2	586	636	1209	65	945	0.131
L09	−125	9.2	639	666	1202	61	936	0.105
L10	−125	13.3	654	673	1188	62	859	0.067
L13	−125	15.5	675	685	1222	62	824	0.046
L15	−125	19.9	700	702	1226	61	784	0.023
L02	−196	3.9	909	—	876	0.3		
L04	−196	8.2	915	—	973	2.5	1278	0.086
L12	−196	10.6	945	—	981	2.0	1060	0.021
L14	−196	16.8	999	—	1051	3.0	1157	0.028
L01	−196	19.0	1004	—	1074	4.7	1153	0.026

ε_{po} = prestrain, σ_y = yield strength, σ_b = tensile strength, σ_f = fracture strength, ψ = reduction of area, K_p = plastic part of constant in formula $\sigma = K\varepsilon^n$, n_p = plastic part of hardening exponent, and—not determined.

Table IV. Properties Measured in Specimens of FG with Various Tensile Prestrains

Number	T (°C)	ε_{po} (Pct)	σ_y (MPa)	σ_b (MPa)	σ_f (MPa)	ψ (Pct)	K_p (MPa)	n_p
L26	14	0	338	573	1114	67	979	0.202
L27	−43	0	371	521	1038	69	762	0.128
L28	−80	0	355	548	1116	69	907	0.190
L31	−110	0	491	610	1244	69	850	0.104
L40	−196	0	841	—	958	7.8	1075	0.048
L29	−125	3.0	556	617	1249	67	906	0.102
L33	−125	4.6	594	648	1263	65	892	0.098
L34	−125	8.5	639	669	1200	60	855	0.067
L38	−125	23.1	770	770	1304	49	850	0.020
L30	−196	2.6	843	—	991	8.8	1054	0.038
L32	−196	4.4	884	—	1036	11.0	1066	0.035
L35	−196	5.9	910	—	1023	6.4	1090	0.030
L37	−196	8.3	950	—	1123	13.4	1099	0.028
L36	−196	12.8	974	—	1062	6.0	1130	0.030

ε_{po} = prestrain, σ_y = yield strength, σ_b = tensile strength, σ_f = fracture strength, ψ = reduction of area, K_p = plastic part of constant in formula $\sigma = K\varepsilon^n$, n_p = plastic part of hardening exponent, and — not determined.

Table V. Parameters Measured on Fracture Surfaces of CG without Prestrain

Number	W (mm)	B (mm)	T (°C)	σ_y (MPa)	ε_{po} (Pct)	X_f (μm)	P_f (kN)	P_{gy}* (kN)	P_f/P_{gy}	σ_{yyc} (MPa)	ε_{pc}	Fib (μm)	Mark
009	12.49	12.50	−100	402	0	280	37.4	18.9	1.978			50	
011	12.55	12.67	−100	402	0	184	22.1	19.5	1.138	1100	0.157	118	L
012	12.4	12.37	−100	402	0	108	30.1	18.3	1.642			85	
018	12.29	12.40	−100	402	0	0	20.0	17.9	1.118	955	0.410	0	L
005	12.55	12.35	−125	469	0	202	11.4	22.1	0.516	878	0.014	0	L
006	12.31	12.55	−125	469	0	0	11.0	21.2	0.519	592	0.023	0	L
007	12.57	12.53	−125	469	0	4	18.0	22.6	0.799	691	0.052	0	L
008	12.41	12.54	−125	469	0	0	19.0	21.7	0.875	716	0.068	0	L
015	12.51	12.39	−125	469	0	0	22.2	22.0	1.009	745	0.137	0	L
017	12.41	12.45	−125	469	0	70	19.8	21.6	0.917	806	0.052	0	L
001	12.29	12.50	−196	793	0	0	11.2	35.5	0.316	937	0.018	0	L
002	12.49	12.65	−196	793	0	0	12.1	37.8	0.322	940	0.018	0	L
003	12.70	12.59	−196	793	0	0	13.0	39.5	0.328	942	0.019	0	L
004	12.17	12.15	−196	793	0	0	11.6	33.5	0.354	947	0.020	0	L
013	12.32	12.44	−196	793	0	65	7.5	35.6	0.211	1027	0.006	0	L
014	12.44	12.43	−196	793	0	0	9.2	36.7	0.251	924	0.012	0	L
016	12.16	12.10	−196	793	0	0	10.8	33.3	0.325	941	0.018	0	L

W = actual height of specimen, B = actual thickness of specimen, T = test temperature, σ_y = yield stress, ε_{po} = prestrain, X_f = distance from cleavage origin to notch tip, P_f/P_{gy} = ratio of fracture load over general yield load, σ_{yyc} = normal tensile stress at cleavage initiating position, ε_{pc} = plastic strain at cleavage initiating position, Fib = length of fibrous crack, and Mark-site of cleavage initiation located at a distance shorter than that of the peak tensile stress designated as L, and otherwise as R.

*The values of P_{gy} were calculated with actual B and $(W - a)$ values, which were measured individually for each specimen with or without prestrain. The notch depth a = 4.25 mm.

C. *Results of FEM Calculations*

The FEM results were assessed by two procedures, as shown in Appendix I.

Typical calculation results of distributions of tensile stress and strains in front of a blunt notch tip are shown in Figure 11. The distance X from notch tip normalized by the tip radius ρ is taken as the abscissa. The ordinates are tensile stress σ_{yy} and strain ε_p. The former is normalized by the yield strength σ_y.

From the calculated distributions of stress and strain and the measured distance of the cleavage initiation site X_f, the tensile stress and strain at X_f can be obtained, and are designated as σ_{yyc} and ε_{pc} in Tables V through VIII. The σ_{yyc} shows a variety of measured values, but there is a minimum value around 600 and 800 MPa for CG and FG steels, respectively. In specimens tested at −100 °C and −125 °C, the ε_{pc} shows a dramatic fluctuation of measured values upward from 0.02. At −196 °C, the values of ε_{pc} are much more stable and show values ranging from 0.01 to 0.02.

IV. DISCUSSION

In this work, for deliberately coarse-grained ferrite-pearlite steel, discussion centers on two interesting phenomena that were observed.

(1) An appreciable drop in notch toughness of specimens that experience 3 pct tensile prestrain. Further prestrain

Table VI. Parameters Measured on Fracture Surfaces of CG with Various Prestrains

Number	W (mm)	B (mm)	T (°C)	σ_y (MPa)	ε_{po} (Pct)	X_f (μm)	P_f (kN)	P_{gy}* (kN)	P_f/P_{gy}	σ_{yyc} (MPa)	ε_{pc}	Fib (μm)	Mark
102	12.17	12.10	−100	514	3.7	0	12.7	21.6	0.589	640	0.035	0	L
113	11.62	11.72	−100	544	4.9	0	11.4	19.2	0.592	678	0.035	0	L
110	11.96	11.64	−100	570	5.7	6	14.8	21.9	0.676	742	0.044	0	L
118	11.76	11.31	−100	520	7.0	0	8.6	18.4	0.466	613	0.023	0	L
109	11.39	11.30	−100	564	8.0	0	11.5	18.0	0.639	715	0.041	0	L
204	11.62	12.01	−100	577	10.0	0	11.2	20.9	0.535	701	0.029	0	L
216	11.73	11.31	−100	616	12.9	0	19.1	21.6	0.884	789	0.110	0	L
201	11.22	11.23	−100	623	13.1	4	11.4	18.9	0.603	775	0.042	0	L
212	11.57	11.37	−100	621	13.7	0	12.7	21.0	0.607	764	0.044	0	L
211	10.81	11.36	−100	648	17.5	6	11.8	17.6	0.672	819	0.051	0	L
214	11.08	10.93	−100	676	22.9	0	8.9	19.1	0.466	814	0.027	0	L
108	12.29	11.93	−125	469	3.1	0	11.5	20.1	0.571	624	0.035	0	L
106	11.92	12.15	−125	540	4.1	0	9.9	21.4	0.462	635	0.024	0	L
116	11.93	12.03	−125	597	6.6	0	9.9	23.5	0.421	701	0.021	0	L
115	11.78	12.02	−125	594	6.7	0	11.2	22.5	0.497	706	0.028	0	L
114	11.53	11.58	−125	590	6.9	0	8.1	20.1	0.405	692	0.020	0	L
111	11.21	11.49	−125	599	7.9	0	10.5	18.5	0.567	733	0.035	0	L
205	11.44	11.80	−125	622	9.7	0	9.8	21.1	0.466	732	0.025	0	L
206	11.67	11.58	−125	646	11.4	0	11.3	22.8	0.495	781	0.032	0	L
218	11.18	11.24	−125	662	12.3	0	11.1	19.8	0.561	808	0.040	0	L
210	11.01	10.98	−125	667	13.7	0	10.1	18.6	0.544	806	0.038	0	L
101	10.31	10.33	−125	679	16.9	0	8.6	14.3	0.601	834	0.046	0	L
203	11.69	11.38	−125	680	18.3	122	7.1	23.8	0.299	1087	0.014	0	L
104	11.94	12.03	−196	884	2.8	16.5	10.1	34.9	0.290	1109	0.016	0	L
103	11.86	12.28	−196	894	3.9	5	6.1	35.3	0.173	1055	0.008	0	L
117	11.70	11.79	−196	908	4.7	0	10.9	33.0	0.329	1093	0.022	0	L
208	11.66	11.66	−196	912	6.2	0	6.4	32.4	0.196	1062	0.010	0	L
213	12.06	11.74	−196	925	6.9	0	8.9	36.8	0.242	1082	0.013	0	L
215	11.53	11.40	−196	937	9.4	0	9.1	31.4	0.289	1085	0.018	0	L
105	11.54	11.42	−196	884	10.8	49	8.0	31.4	0.253	1207	0.012	0	L
217	11.33	11.31	−196	958	11.5	0	5.3	30.1	0.177	1117	0.009	0	L
209	11.29	11.07	−196	957	15.0	0	6.7	30.8	0.218	1125	0.011	0	L
207	11.19	11.02	−196	991	15.6	0	5.1	29.2	0.176	1155	0.009	0	L
202	11.33	11.11	−196	988	18.2	41	7.7	30.8	0.250	1317	0.016	0	L

up to 20 pct has a negligible effect on toughness even though the yield strength still increases.

(2) The majority of zero values of X_f, the distance from the cleavage initiating site to the notch tip, are found in specimens that experience prestrain.

A. *Critical Event for Cleavage*

The critical event, being the controlling link in the mechanism of cleavage, is the most difficult step among the three consecutive steps of the cleavage process; *i.e.*, crack nucleation in a second-phase particle, the just-nucleated crack passing through the boundary between the second-phase particle and the matrix grain, and the propagation of the grain-sized crack across the grain boundary. Crack nucleation was taken as the critical event before the early 1950s.[31] From the 1960s, the concept of crack nucleation controlled by plastic strain was replaced by crack propagation of the nucleated crack controlled by tensile stress as the critical event for cleavage.[18,32] At the moderate low temperature, it is widely realized that the propagation of crack controlled by tensile stress σ_{yy} is the critical event. However, recently, a dual criterion for cleavage of notched specimens, *i.e.*, a critical plastic strain ($\varepsilon_p \geq \varepsilon_{pc}$) for nucleating a crack and a critical tensile stress ($\sigma_{yy} \geq \sigma_f$) for its propagation, has been suggested again.[11,12,24,25,30,33] Previously, Oates and Griffiths,[13] Lin *et al.*,[14] and the present authors[15] suggested that the critical event can be changed from the propagation of a grain-sized crack to the propagation of a second-phase particle-sized crack to the nucleation of a crack by increasing the acuity of the test specimen defect or decreasing the test temperature. These works suggest that the critical event for cleavage can be changed with the variation of the test environment.

One characteristic feature showing a tensile stress-controlling crack propagation mechanism is cracks failing to propagate and remaining in a fractured specimen; these microcracks can be observed in the metallographic section perpendicular to the fracture notch. Doubly notched specimens are particularly appropriate for observing the remaining cracks in front of the surviving notch after the specimen is fractured at one notch. That a crack remains in front of the surviving notch means the tensile stress was not sufficient to propagate the crack just nucleated. Fibrous cracking occurring before cleavage initiation is also an indication of insufficient tensile stress to propagate a nucleated crack in a cleavage manner.

One characteristic feature of strain-controlled nucleation mechanism is that the site of cleavage initiation is located at a distance closer to the notch tip than that of the peak tensile stress (marked L in Tables V through VIII), where

Table VII. Parameters Measured on Fracture Surfaces of FG without Prestrains

Number	W (mm)	B (mm)	T (°C)	σ_y (MPa)	ε_{po} (Pct)	X_f (μm)	P_f (kN)	P_{gy} (kN)	P_f/P_{gy}	σ_{yyc} (MPa)	ε_{pc}	Fib (μm)	Mark
503	12.91	12.86	−125	494	0	0	28.2	24.5	1.151	940	0.197	10∼20	L
504	12.97	12.97	−125	494	0	0	38.3	27.0	1.418	1118	0.999	0	L
505	12.86	12.89	−125	494	0	0	34.4	26.0	1.323	1051	0.563	20∼40	L
601	12.93	12.94	−125	494	0	0	37.7	26.7	1.413	1114	0.969	0	L
602	12.93	12.87	−125	494	0	745	42.0	26.5	1.589	1726	0.032	120	R
603	12.95	12.95	−125	494	0	0	26.9	26.9	0.999	865	0.097	0	L
604	12.92	12.92	−125	494	0	349	34.2	24.5	1.396	1664	0.041	0	R
502	12.98	12.92	−196	843	0	0	15.0	46.0	0.326	1027	0.019	0	L
506	12.83	12.87	−196	843	0	96	13.9	44.3	0.314	1345	0.008	0	L
507	12.97	12.98	−196	843	0	10	16.4	46.1	0.355	1090	0.198	0	L
508	12.91	12.93	−196	843	0	0	20.8	45.4	0.458	1060	0.330	0	L
509	12.93	12.95	−196	843	0	0	17.5	45.7	0.384	1043	0.248	0	L
510	12.84	12.83	−196	843	0	0	14.8	44.3	0.334	1031	0.197	0	L
605	12.96	12.95	−196	843	0	0	33.1	46.0	0.721	1111	0.076	0	L

Table VIII. Parameters Measured on Fracture Surfaces of FG with Various Prestrains

Number	W (mm)	B (mm)	T (°C)	σ_y (MPa)	ε_{po} (Pct)	X_f (μm)	P_f (kN)	P_{gy} (kN)	P_f/P_{gy}	σ_{yyc} (MPa)	ε_{pc}	Fib (μm)	Mark
609	12.68	12.64	−125	539	3.3	0	22.7	26.9	0.844	787	0.075	0	L
607	12.53	12.48	−125	587	5.2	0	27.9	27.9	0.999	852	0.147	0	L
701	12.50	12.46	−125	621	6.8	0	29.2	29.3	0.997	894	0.180	0	L
606	12.47	12.38	−125	649	8.4	254	23.7	30.2	0.785	1311	0.019	0	L
705	11.93	11.98	−125	722	14.5	0	19.4	28.3	0.686	935	0.060	0	L
704	12.03	11.98	−125	725	14.9	0	21.9	29.2	0.750	939	0.073	0	L
710	11.76	11.88	−125	752	19.0	20	24.5	27.7	0.884	1248	0.059	0	L
709	11.66	11.74	−125	759	20.5	0	13.7	27.0	0.508	921	0.035	0	L
608	12.77	12.76	−196	858	2.7	8	14.9	44.0	0.338	1147	0.020	0	L
610	12.56	12.76	−196	899	5.2	0	9.0	43.6	0.207	1053	0.010	0	L
702	12.32	12.50	−196	931	7.7	0	11.8	41.9	0.280	1085	0.016	0	L
706	12.47	12.38	−196	979	14.0	3	8.1	40.2	0.201	1146	0.010	0	L
707	12.53	12.48	−196	993	17.1	0	8.3	37.9	0.220	1174	0.012	0	L
708	12.77	12.76	−196	993	17.2	0	7.5	38.1	0.198	1162	0.011	0	L
703	11.67	11.58	−196	1002	20.2	0	9.3	35.8	0.260	1193	0.016	0	L

the plastic strain is sufficient to nucleate a crack.[16] Strictly speaking, the feature is that the number fraction of this site (marked L) is much higher than that of the site located at a distance farther than that of peak stress (marked R).

1. *Critical event for cleavage of specimens without prestrain*

In this work, it is found in Table V that at the test temperature of −100 °C, among four specimens of CG without prestrain, fibrous cracks developed before cleavage in three specimens. However, in one specimen, the cleavage initiated at the notch tip and propagated directly at an applied load higher than the general yield load. These facts mean that the crack-propagation model dominates the cleavage fracture, but there is the possibility of nucleation-controlled fracture.

For CG specimens without prestrain tested at −125 °C, no fibrous cracking was observed and in four specimens, the cleavage initiated at or very close to the notch tip, suggesting the nucleation-controlling mechanism. However, in one doubly notched specimen (017, Figure 10(a)), a grain-sized crack stemming from the surviving notch tip remains, indicating that the critical event is propagation of a grain-sized crack controlled by tensile stress. Therefore, a mixed mechanism of cleavage, under a critical mechanical condition, appears in this group with a greater tendency for nucleation controlled than at −100 °C.

From Table VII, the cleavage mechanism of FG specimen without prestrain at −125 °C behaves similarly to that of the CG specimen at −100 °C. Fibrous cracks occur and extend in three specimens, and in one doubly notched specimen (604, Figure 10(b)), a pearlite colony-sized crack remains in front of the surviving notch, indicating the propagation-controlling mechanism. In other specimens, the cleavage initiates at the notch tip and propagates directly at an applied load higher than the general yield load. This means the dominant cleavage mechanism is propagation of a nucleated crack controlled by tensile stress with a stronger tendency of transferring to nucleation-controlled fracture.

For both CG and FG specimens tested at −196 °C, the dominant mechanism is nucleation controlled.

2. *Critical event for cleavage of specimens with prestrain*

From Tables VI and VIII, it is found that among 49 specimens with various prestrains, for the majority (45) of specimens, the cleavage initiates at $X_f = 0$ or very close to the notch tip. However, it is well established for con-

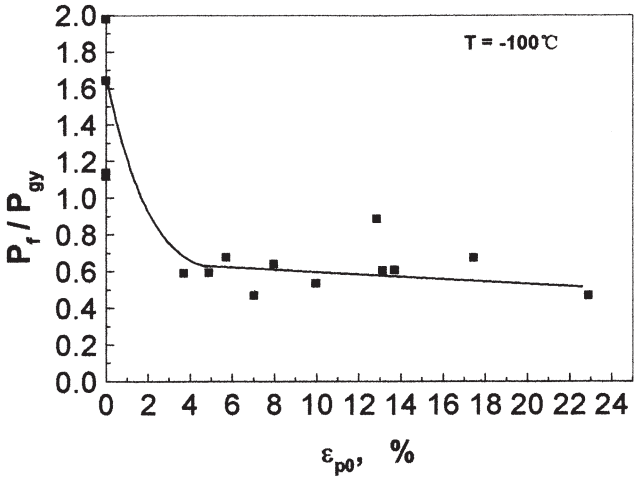

(*a*)

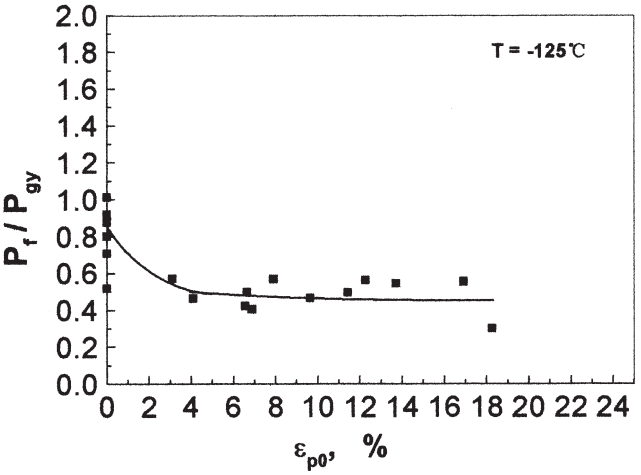

(*b*)

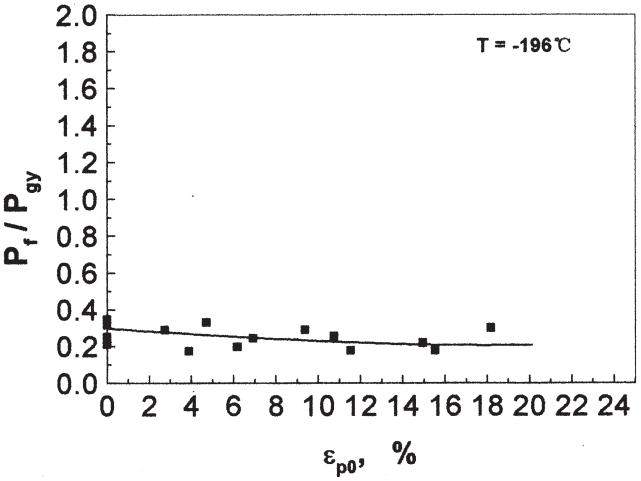

(*c*)

Fig. 7—Variations of notch toughness at various test temperatures plotted against the prestrains for CG (*a*) −100 °C, (*b*) −125 °C, and (*c*) −196 °C.

ventional ferrite-pearlite steel with grain sizes of 10 to 30 μm tested at moderately low temperature that cleavage is always initiated at a distance more than 300 μm in front of the notch tip.[17]

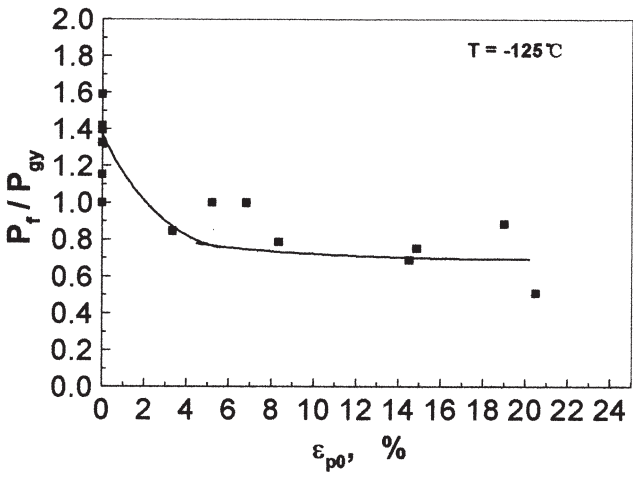

(*a*)

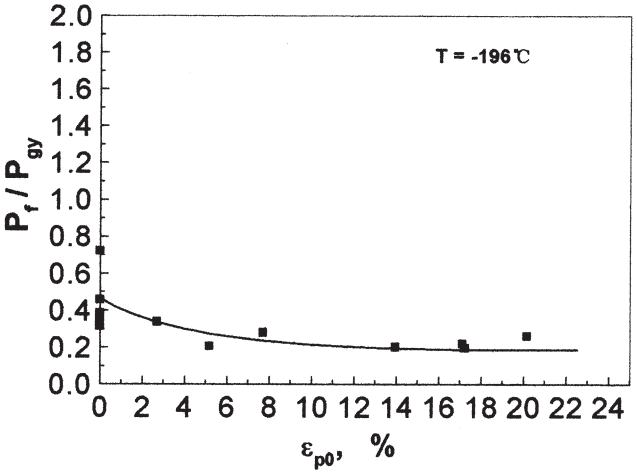

(*b*)

Fig. 8—Variations of notch toughness at various test temperatures plotted against the prestrains for FG (*a*) −125 °C and (*b*) −196 °C.

The phenomenon of "zero distance X_f" in this work is considered to be caused by two events. First, very large grain sizes (up to 160 μm) result in a very low local fracture stress σ_f. As found in Tables V through VIII, minimum values of critical σ_{yyc} around 600 and 800 MPa are measured for CG and FG, respectively. Therefore, it is possible for the tensile stress just at the notch tip σ_{yyt}, much less than the peak value, to exceed the σ_f and to propagate a just nucleated crack at the tip. Second, the steel used is very clean with carbon content of 0.06 pct and sulfur content of 0.009 pct. Most critical plastic strains ε_{pc} measured at −100 °C to −125 °C are higher than 0.02. It is difficult to nucleate a crack at a distance in front of the notch where the ε_p is lower.

The fact that the cleavage initiates at the tip of the notch, a site subjected to the highest plastic strain and less tensile stress, characterizes the nucleation-controlled critical event. The lower local fracture stress σ_f and higher critical plastic strain ε_{pc} of the coarse microstructures facilitate the nucleation-controlled mechanism.

No fibrous cracking and no remaining cracks were found in the specimens that received the prestrain. These facts also support the nucleation-controlled mechanism.

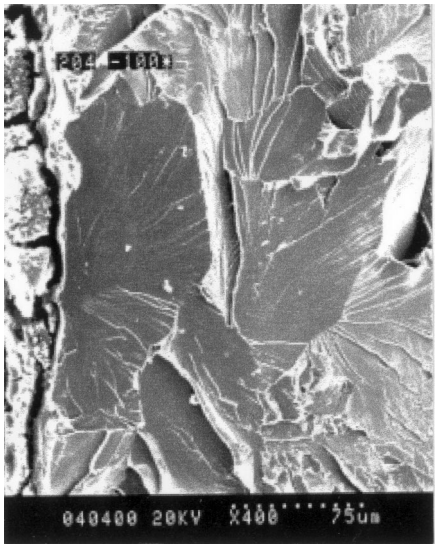

(*a*)

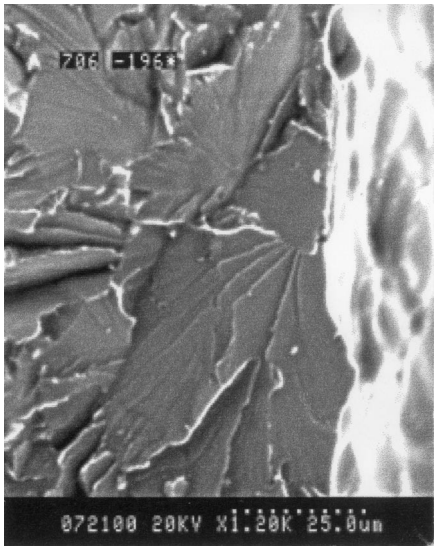

(*b*)

Fig. 9—Typical fracture surface of specimens with prestrain (*a*) CG with ε_{po} = 9.97 pct, X_f = 0, and T = −100 °C; and (*b*) FG with ε_{po} = 13.97 pct, X_f = 3 μm, and T = −196 °C.

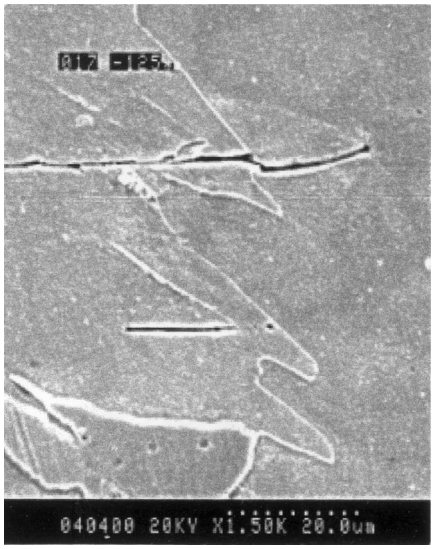

(*a*)

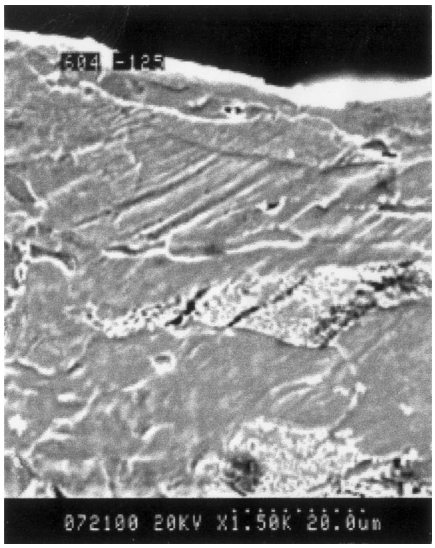

(*b*)

Fig. 10—Grain size (CG with ε_{po} = 0, T = −125 °C) (*a*) and pearlite colony-size (FG with ε_{po} = 0, T = −125 °C) (*b*) Remaining microscopic cracks found in front of the survived notch of fractured doubly notched specimens.

3. Change of critical event by prestraining

As indicated in Sections IV–A–1 and 2, the cleavage shows a dominant propagation-controlled mechanism for specimens without prestrain, yet a nucleation-controlled mechanism for specimens with various prestrains. The driving force that causes the change in cleavage mechanism is analyzed as follows: Figure 12(a) shows the case of conventional steel for which at the notch tip the accumulated plastic strain ε_p exceeds the ε_{pc} and a crack could be nucleated, but the tensile stress is insufficient. Cleavage cannot be propagated at the notch tip directly. In the case where the ε_{pc1} is low, within a distance X_2 from the notch tip, the ε_p is sufficient to nucleate a crack but the σ_{yy} is insufficient to propagate it in the region between X_1 and X_2; thus, the cleavage is controlled by crack propagation in this region. In the case where the ε_{pc2} is high, within a distance X_1, the tensile stress σ_{yy} is sufficient to propagate a crack but the ε_p is insufficient to nucleate a crack in the region between X_1 and X_3; thus, the cleavage is controlled by crack nucleation in this region. This process shows the possibility of a dual-criterion cleavage process.[12]

Figure 12(b) shows the case of insufficient tensile stress, which is lower than the σ_f and fails to propagate a just-nucleated crack. A fibrous crack develops or a nucleated crack failing to extend remains in the specimen. The process shows the propagation-controlled mechanism. This is the case that occurs in most specimens without prestrain tested at −100 °C to −125 °C.

Figure 12(c) shows the case of lower σ_f and higher ε_{pc}. At the tip of the notch, the σ_{yy1} is sufficient to exceed

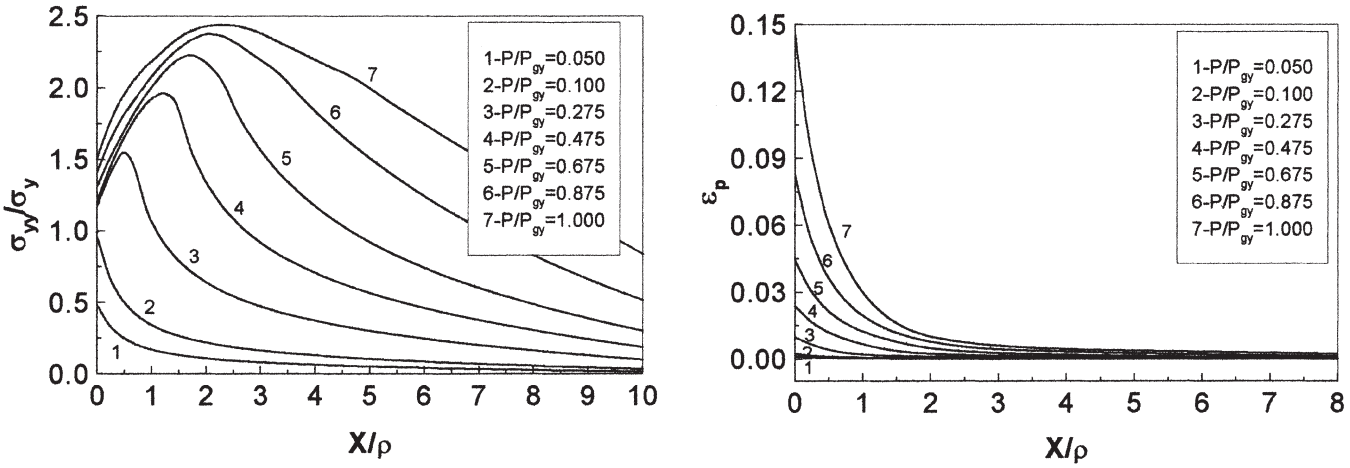

Fig. 11—Distributions of tensile stress and strain in front of a blunted notch calculated by ABAQUS code with power law of work hardening $n_p = 0.098$, $\sigma_y/E = 1/300$.

the σ_f, but the plastic strain ε_{p1} is insufficient to exceed the ε_{pc}, so no crack initiates. With further increase of the applied load, the plastic strain accumulated at the notch tip increases to ε_{p2} and exceeds ε_{pc}, and a crack nucleates and propagates. The process shows the nucleation-controlled mechanism. This is the case in specimens with various prestrains.

Table IX gives a summary of the comparison of parameters of specimens with and without prestrain. In Table IX, the minimum σ_{yyc} in Tables V through VIII is taken as the σ_f. The reason will be addressed in Section IV–B. The σ_{flow} is taken at the plastic strain of ε_{pc}. The stress intensification coefficient $Q = \sigma_m/\sigma_e + 0.577$ at the tip of notch is taken as 1.15 (σ_m/σ_e shows the stress triaxiality). Here, the normal tensile stress at the notch tip $\sigma_{yyt} = Q\sigma_{\text{flow}}$.

Table IX reveals that in specimens of CG, which do not experience prestrain and are tested at −100 °C, the propagation-controlled critical event results when the tensile stress σ_{yyt} fails to reach the σ_f at the notch tip, where the plastic strain reaches its critical value ε_{pc} of 0.02. However, the difference between σ_{yy} and σ_f is small. For specimens tested at −125 °C, the σ_{yyt} just reaches the σ_f, and a mixed mechanism operates. In both cases, a slight increase in σ_{yyt} can play a key role in the change of the critical event.

In Table IX, an increase of 90 and ~60 MPa in σ_y by 3 pct prestrain for −100 °C and −125 °C, respectively, is just sufficient to cause σ_{yyt} to exceed σ_f at the notch tip and to make the cleavage crack nucleation controlled in CG specimens. Further increasing the prestrain has no effect on the nucleation-controlling critical event. The effect of 3 pct prestrain to increase σ_y by ~70 MPa for FG specimens plays a similar role as for the CG specimens.

4. Effect of temperature

A decrease of temperature raises the yield strength, the effect of which is the same as prestrain to increase the σ_{yyt} at the notch tip.

For all specimens tested at −196 °C, with or without prestrain, the σ_{yyt} exceeds the σ_f, showing a nucleation-controlled cleavage mechanism.

For CG specimens without prestrain tested at −125 °C, the σ_{yyt} reaches σ_f and a mixed mechanism behaves with a stronger nucleation-controlled tendency than that found in specimens tested at −100 °C.

5. Effect of grain size

From Figures 2 and 4, the size of the coarsest grains in CG is around 160 μm and that of FG is around 70 μm. A difference of 90 μm in grain size results in a 50 MPa difference in yield strength at around room temperature. The local fracture stress σ_f measured as the minimum σ_{yyc} is around 600 and 800 MPa for CG and FG, respectively. These figures are perfectly consistent with those results arranged by Curry[21] and summarized by Miyata *et al.*[22]

In spite of an increase of 50 MPa in the yield strength, an increase of 200 MPa in the local fracture stress σ_f of FG has an apparent effect on the critical event. At −100 °C, for FG specimens without prestrain, cleavage fracture cannot occur without a fibrous crack occurring prior to it, indicating a perfect crack-propagation-controlled model. For FG specimens without prestrain tested at −125 °C, the crack-propagation-controlled tendency is much more apparent than that for CG specimens. The effect of the finer grain size of FG on the critical event causes a remarkable increase of notch toughness tested at −125 °C (comparing Figures 7(b) and 8(a)).

B. Analyses of Fluctuation of syyc

A great number of works find that the local fracture stress σ_f is a very stable parameter and is an intrinsic property of steel.[17–20] The σ_f is determined as the value of tensile stress σ_{yyc} at the cleavage initiation site X_f, which is measured at the fracture load. In previous work, most values of σ_f are measured for steels with the crack-propagation mechanism of cleavage controlled by tensile stress. In this case, as shown in Figure 12(a), at a distance between X_1 and X_2, for a lower ε_{pc1}, a crack can be initiated but cannot propagate. With increasing applied load, the front side of the σ_{yy} curve moves forward and makes the σ_{yy} reach the σ_f at a site of a crack just nucleated, and the cleavage occurs. The measured σ_{yy} is the value of σ_f.

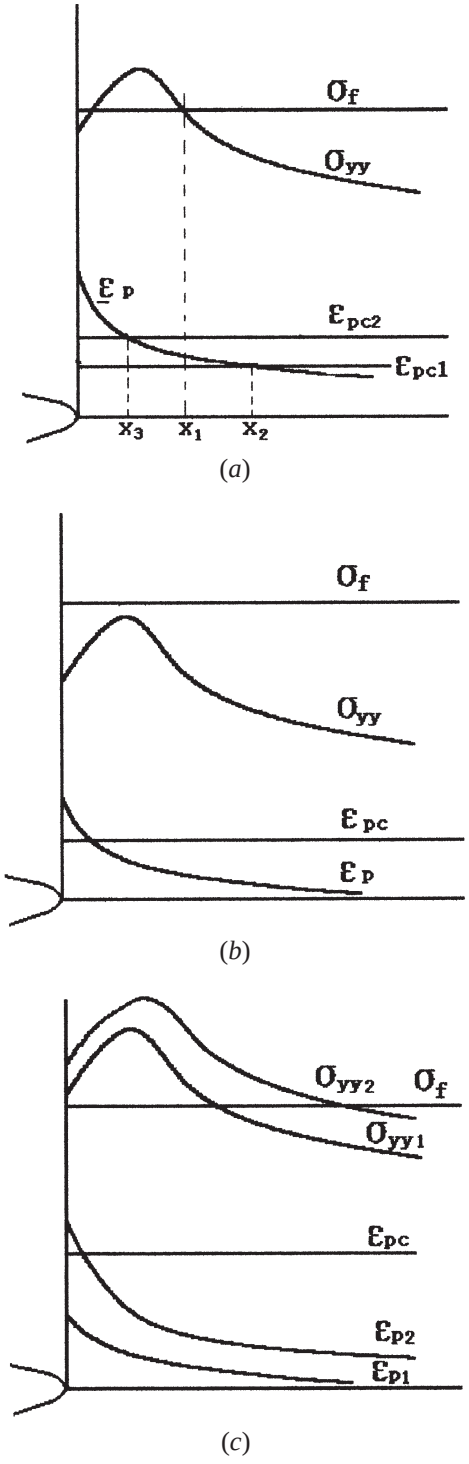

Fig. 12—Schematics of various cleavage models.

However, in the case of crack-nucleation-controlled mechanism, as shown in Figure 12(c), the σ_{yy1} exceeds the σ_f over a distance but the ε_{p1} is insufficient to nucleate a crack. With increasing applied load, the accumulated plastic strain increases to ε_{p2} and a crack nucleates at a site within the distance where ε_{p2} exceeds ε_{pc}. The cleavage occurs at a site where the σ_{yy2} is much higher than the σ_f. This is the case for most measurements in this work. The measured values of σ_{yyc} show a remarkable fluctuation with the fluctuation of ε_{pc} and are much higher than the real σ_f. At the test temperature of −196 °C, the ε_{pc} is stable; correspondingly, the measured values of σ_{yyc} are stable but still much higher than the real σ_f.

In this work, the minimum value of σ_{yyc} is taken as the σ_f. A minimum value of 592 MPa for CG in Table V corresponding to a value of 0.023 of ε_{pc} is more reasonable. The minimum value of 787 MPa for FG in Table VIII, corresponding to a value of 0.075 of ε_{pc}, maybe is slightly higher than the real value but does not affect the analyses. In our previous work,[9,10] it was found that a prestrain up to 20 pct did not affect the values of the local fracture stress σ_f. In Sections A–1 through 5, 600 and 800 MPa are adopted as σ_f for CG and FG, respectively.

C. Effects of Prestrain on the Notch Toughness

From Figure 7, an appreciable drop in notch toughness (characterized by P_f/P_{gy}) is found in CG specimens tested at −100 °C and −125 °C, which experience 3 pct tensile prestrain. Further prestrain has negligible effect on toughness. But for those tested at −125 °C, the difference between specimens without prestrain and specimens with prestrain is reduced, and two values of notch toughness of the former (005, 006 in Table V) drop into the range of the latter. This behavior in toughness is consistent with the variation of the critical event for cleavage. For CG specimens tested at −100 °C, an increase of 90 MPa in yield strength σ_y by around 3 pct prestrain causes the change from crack propagation controlled to crack nucleation controlled and the fracture load P_f decreases. Further increase in σ_y by prestrain up to 20 pct does not affect the critical event and does not affect the toughness. For CG specimens without prestrain tested at −125 °C, an increase in σ_y of ~60 MPa by reducing temperature from −100 °C makes the σ_{yyt} close to σ_f and makes the critical event mixed. Therefore, the behavior of toughness also presents a mixed mode in Figure 7(b). Prestrain facilitates further the nucleation mechanism and a low value of toughness. For FG specimens tested at −125 °C (Figure 8(a)), the variation of the critical event and related toughness corresponds to CG specimens tested at −100 °C and −125 °C. The effect of prestrain on the notch toughness has similar effects.

Due to the high yield stress, all specimens tested at −196 °C, without or with prestrain, show nucleation-controlled cleavage and the difference in the notch toughness is reduced and obscured by the scatter of the measured values.

V. SUMMARY

From this work of 4PB tests of notched prestrained steel specimens with deliberately coarsened grains, combining the microscopic observation and FEM calculations, the following conclusions can be drawn.

1. An appreciable decrease in notch toughness is induced in specimens that experience 3 pct tensile prestrain and are tested at −100 °C and −125 °C. Further prestrain has a negligible effect on toughness even though it still increases the yield strength.

Table IX. Comparison of Parameters of Specimens without and with Prestrain

Microstructure	T (°C)	ε_{po} (Pct)	σ_y (MPa)	ε_{pc}	σ_{flow} (MPa)	Q	σ_{yyt} (MPa)	σ_f (MPa)	Note
CG	−100	0	402	0.02	465	1.15	535	592	$\sigma_{yyt} < \sigma_f$
CG	−100	3.7	512	0.02	545	1.15	626	592	$\sigma_{yyt} > \sigma_f$
CG	−125	0	469	0.02	510	1.15	586	592	$\sigma_{yyt} \approx \sigma_f$
CG	−125	3.1	533	0.02	562	1.15	646	592	$\sigma_{yyt} > \sigma_f$
CG	−196	0	793	0.01	810	1.15	931	592	$\sigma_{yyt} > \sigma_f$
FG	−125	0	494	0.03	555	1.15	638	787	$\sigma_{yyt} < \sigma_f$
FG	−125	3.3	561	0.075	675	1.15	776	787	$\sigma_{yyt} \approx \sigma_f$
FG	−196	0	842	0.01	850	1.15	977	787	$\sigma_{yyt} > \sigma_f$

T = test temperature, ε_{po} = prestrain, σ_y = yield strength, ε_{pc} = critical plastic strain, σ_{flow} = flow stress, Q = stress intensification coefficient at notch tip caused by stress triaxiality, $\sigma_{yyt} = Q\sigma_{\text{flow}}$ tensile stress at notch tip, and σ_f = local fracture stress.

The effect of prestrain on the notch toughness at −196 °C is negligible.

2. The decrease of toughness results from a change in the critical event controlling the cleavage fracture. An increase of the yield strength in the prestrained specimens facilitates the critical event changing from the propagation of a nucleated microcrack to the nucleation of the microcrack and then deteriorates the toughness. An increase of yield strength by decreasing test temperature acts in the same way.
3. The local fracture stress σ_f is an intrinsic property of steel. However, only for the condition that cleavage is controlled by the crack propagation mechanism will the values determined as the normal tensile stress σ_{yyc} at the cleavage initiation site X_f be stable. Otherwise, in the condition of crack-nucleation-controlled cleavage, the measured values of σ_{yyc} present a great variety. A minimum value of σ_{yyc} can be taken as the σ_f.

ACKNOWLEDGMENTS

This work was financially supported by the National Natural Science Foundation of China (Grant No. 59871015) and the Key Research and Development Program for Outstanding Group of Gansu University of Technology. The authors thank Miss Wang Qing and Miss Cao Rui for their help in arranging the pictures and calculations.

APPENDIX I

The distribution of the mesh around the notch root used in the ABAQUS calculations is shown in Figure Ia. According to the suggestion of Griffiths and Owen's work,[28] the FEM calculation using the ABAQUS code was assessed by two procedures. The first is comparing the spreading length of the plastic zone in front of the notch root, calculated by this work and measured by Griffiths and Oates' experiments.[13] The second is comparing the convergence results calculated using a coarse mesh and a fine mesh. The results are presented in Figure Ib. It can be seen that the results calculated by a coarse mesh and a fine mesh are consistent with each other. Both match the experimental results obtained by Griffiths and Oates. Although the work hardening rate of the experimental materials is different, it has a negligible effect on the plastic zone spread. Figure Ic presents the plastic zone

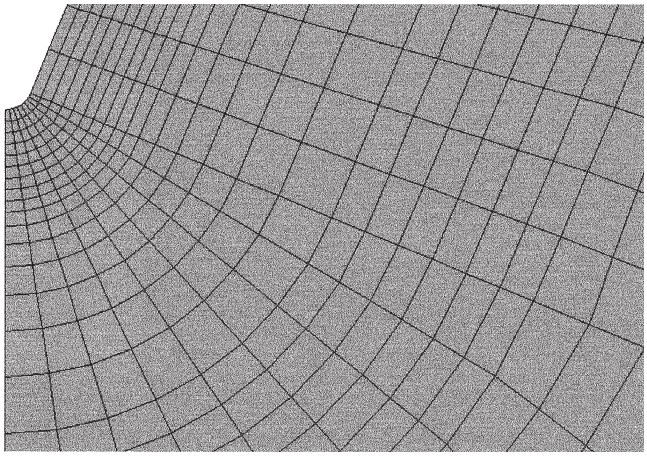

Fig. Ia—The distribution of mesh around the notch root.

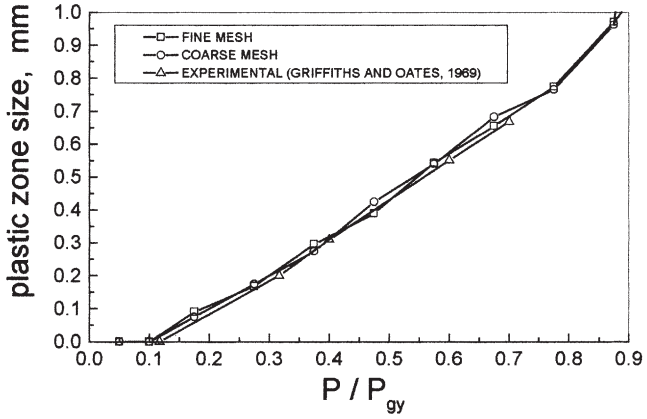

Fig. Ib—Comparison of spreading sizes of plastic zones in front of notch roots calculated and measured by experiments.

spreading in specimens with different prestrains at various applied loads. Based on these comparisons, it is considered that the FEM calculation can support the conclusions of this article. In the legend of Figure Ic, P_{gy} is determined by the applied load at which a plastic "hinge" spreads across the notched cross section to leave an elastic enclave located on the symmetry axis.[28] Putting the values of P_{gy} into the formula presented in Section II–C–2, the calcu-

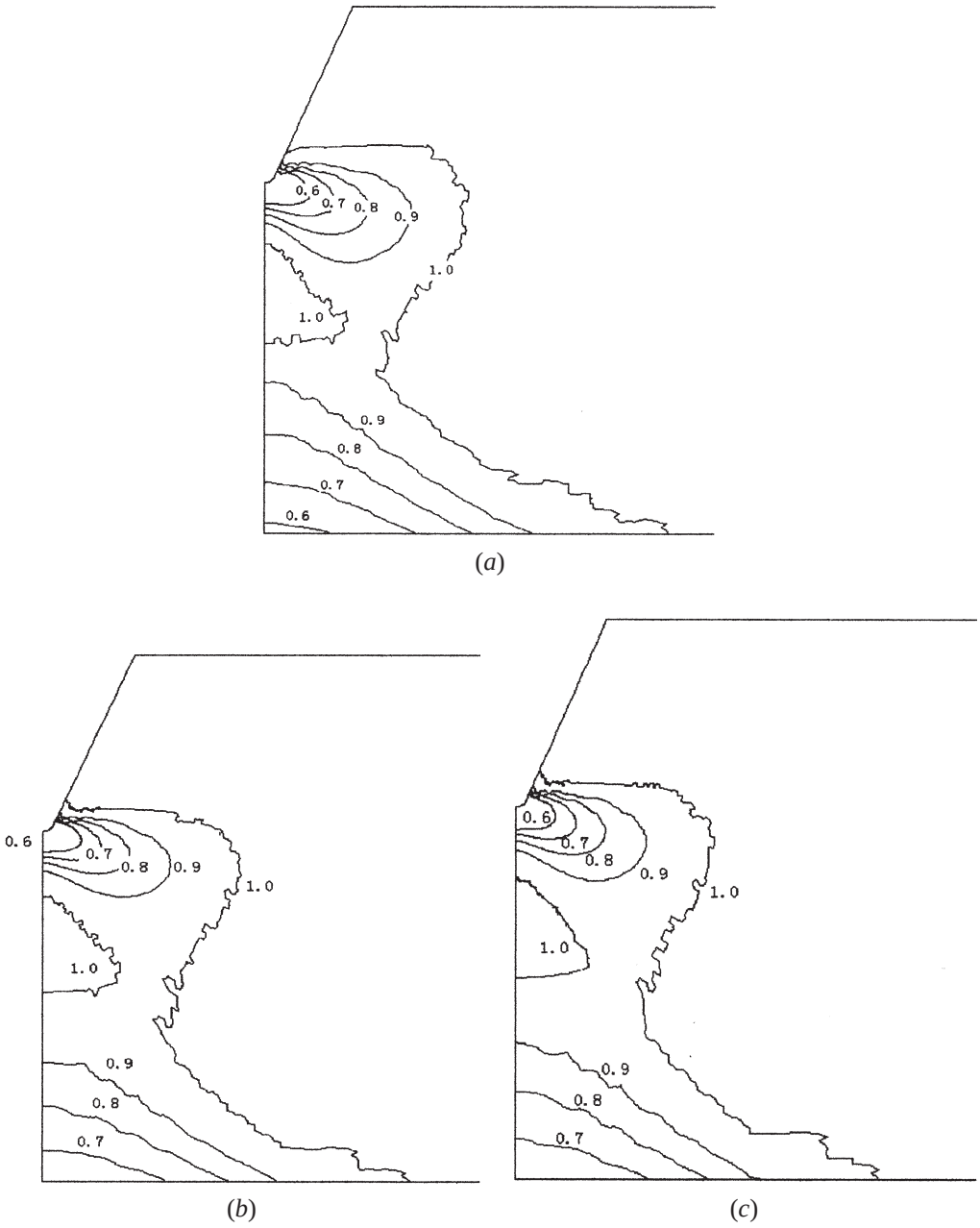

Fig. Ic—Plastic zone development at notch with different prestrains: (*a*) $\varepsilon_{po} = 0$, $P_{gy} = 25.7$ kN; (*b*) $\varepsilon_{po} = 8$ pct, $P_{gy} = 32.7$ kN; and (*c*) $\varepsilon_{po} = 18$ pct, $P_{gy} = 38$ kN. Figures show the values of P/P_{GY}.

lated constraint factors are 1.26, 1.22, and 1.23 for $\varepsilon_{po} = 0$, $\varepsilon_{po} = 8$ pct, and $\varepsilon_{po} = 18$ pct, respectively. The differences between these values and the value 1.22 adopted in the formula are small; therefore, the constraint factor 1.22 is reasonable. The prestrain has little effect on the constraint factor.

APPENDIX II

Figure IIa compares the results calculated with original specimen dimensions (shown in Figure 5(a)) and with specimen dimensions after 20.5 pct prestrain (no. 709). It is found that in the condition of using a parameter of P/P_{gy}, the variation in specimen dimensions gives a negligible effect on the calculated values of strain distribution (Figure II(b)). For normal stress distribution at sites left (shorter distance from the precrack tip) to the sites where the maximum normal stress locates, the effect of geometry variations is also negligible. As seen in Tables V through VIII, in most cases, the cleavage is triggered at locations left of the sites where the maximum normal stress is located (marked by L in the last column of the tables). Thus, the original specimen's dimensions shown in Figure 5(a) were used for FEM calculations throughout this work.

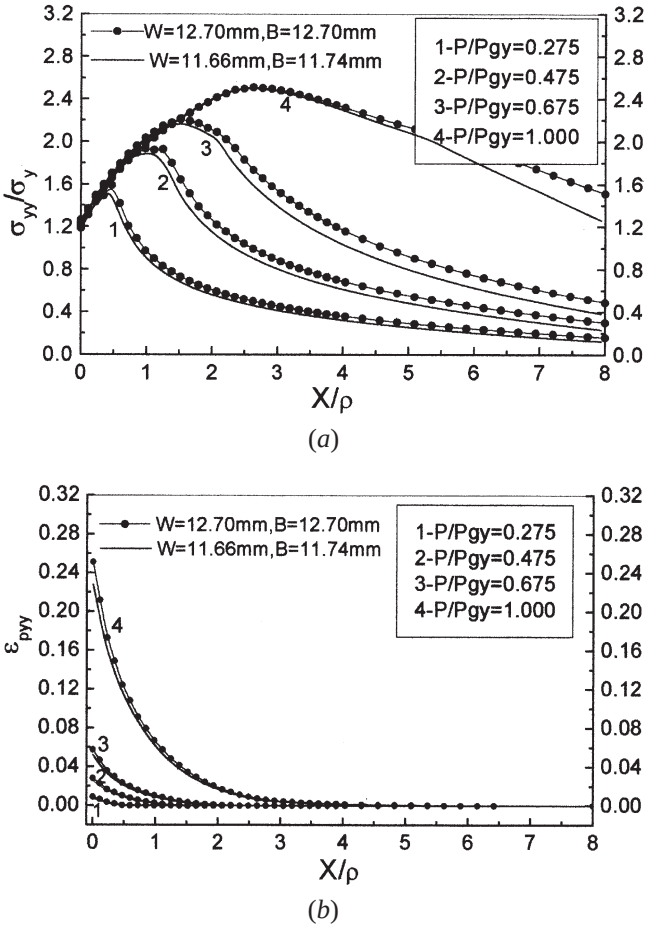

Fig. IIa—Comparison of results calculated with specimen of original dimensions and with specimen subjected to a 20.5 pct tensile prestrain (no. 709): (*a*) normal stress distribution and (*b*) strain distribution.

REFERENCES

1. C.J. Osborn, A.F. Scotchbrook, R.D. Stout, and B.G. Johnston: *Welding J.*, 1949, vol. 28, pp. 337s-53s.
2. E.J. Ripling and W.M. Baldwin, Jr.: *Trans. ASM*, 1951, vol. 43, pp. 778-810.
3. F.W. Bridgman: in *Studies in Large Plastic Flow and Fracture*, Part III, McGraw-Hill, New York, NY, 1952, pp. 293-338.
4. W.T. Lankford: *Welding J.*, 1956, vol. 35, pp. 195s-206s.
5. G.E. Turner: *J. Iron Steel Inst.*, 1961, vol. 197, pp. 131-35.
6. J. Dvorak: *Welding J.*, 1966, vol. 45, pp. 235s-40s.
7. N.J. Petch and R.W. Armstrong: *Acta Metall.*, 1989, vol. 37, pp. 2279-85.
8. P.M. Lorenz: *Trans. ASM*, 1961, vol. 54, pp. 466-80.
9. J.H. Chen, V.B. Wang, G.Z. Wang, and X. Chen: *Eng. Fract. Mech.*, 2001, vol. 68, pp. 1669-86.
10. J.H. Chen, H.J. Wang, G.Z. Wang, Z.Q. Dong, and X. Chen: *Int. J. Fract.*, 2002, vol. 117, pp. 375-92.
11. M.G. Mendiratta, R.L. Goetz, and D.M. Dimiduk: *Metall. Mater. Trans. A*, 1996, vol. 27A, pp. 3903-12.
12. G.Z. Wang and J.H. Chen: *Int. J. Fract.*, 1998, vol. 89 (3), pp. 269-84.
13. G. Oates and J.R. Griffiths: *Met. Sci. J.*, 1969, vol. 3 pp. 111-15.
14. T. Lin, A.G. Evans, and R.O. Ritchie: *J. Mech. Phys. Solids*, 1986, vol. 34, pp. 477-97.
15. J.H. Chen, G.Z. Wang, and H. Ma: *Metall. Trans. A*, 1990, vol. 21A, pp. 321-30.
16. G.Z. Wang and J.H. Chen: *Int. J. Fract.*, 2001, vol. 108 (3), pp. 235-50.
17. J.H. Chen, L. Zhu, and H. Ma: *Acta Metall. Mater. A*, 1990, vol. 38, pp. 2527-35.
18. J.F. Knott, *J. Iron Steel Inst.*, 1966, vol. 104, pp. 104-11.
19. A.S. Tetelman, T.R. Wilshaw, and C.A. Rau, Jr.: *Int. J. Fract. Mech.*, 1968, vol. 4, pp. 147-57.
20. J.H. Chen, X.J. Hu, and G.Z. Wang: *Fatigue Fract. Eng. Mater. Struct.*, 1996, vol. 19, pp. 807-19.
21. D.A. Curry: *Met. Sci.*, 1980, vol. 14, pp. 319-23.
22. T. Miyata, R.C. Yang, A. Otsuka, T. Haze, and S. Ahira: *Advances in Fracture Research*, Proc. ICF6, 1989, K Salama, K. Ravi-Chander, R. Taplin, and P. Rama Rao, eds., pp. 2563-72.
23. J.H. Chen, Y. Kikuta, T. Araki, M. Yoneda, and Y. Matsuda: *Acta Metall.*, 1984, vol. 32, pp. 1779-88.
24. J.J. Lewandowski and A.W. Thompson: *Metall. Trans. A*, 1986, vol. 17A, pp. 1769-86.
25. J.J. Lewandowski and A.W. Thompson: *Metall. Trans. A*, 1986, vol. 17A, pp. 461-72.
26. D.J. Alexander and I.M. Bernstein: *Metall. Trans. A*, 1989, vol. 20A, pp. 2321-35.
27. A.V. Samant and J.J. Lewandowski: *Metall. Mater. Trans. A*, 1997, vol. 28A, pp. 398-99.
28. J.R. Griffiths and D.R.J. Owen: *J. Mech. Phys. Solids*, 1971, vol. 19, pp. 419-31.
29. D.J. Alexander, J.J. Lewandowski, W.J. Sisak, and A.W. Thompson: *J. Mech. Phys. Solids*, 1986, vol. 34, pp. 433-54.
30. J.J. Lewandowski and A.W. Thompson: *Acta. Metall.*, 1987, vol. 35(7), pp. 1453-66.
31. A.N. Stroh: *Proceedings*, Royal Society, New York, 1954, A233, pp. 400-32.
32. J.A. Hendrickson: *Trans. ASM*, 1958, vol. 50, pp. 656-76.
33. A.W. Thompson and J.F. Knott: *Metall. Trans. A*, 1993, vol. 24A, pp. 523-34.